Proceedings of the 2018 Design of Medical Devices Conference
DMD2018
April 9-12, 2018, Minneapolis, MN, USA

DMD2018-6804

SOLID-LATTICE HIP PROSTHESIS DESIGN: APPLYING TOPOLOGY AND LATTICE OPTIMIZATION TO REDUCE STRESS SHIELDING FROM HIP IMPLANTS

Yuhao He
Altair ProductDesign, Inc.
Irvine, California, USA

Drew Burkhalter
Altair ProductDesign, Inc.
Irvine, California, USA

David Durocher
Altair Engineering, Inc.
Bothell, Washington, USA

James M. Gilbert
Altair ProductDesign, Inc.
Bothell, Washington, USA

ABSTRACT

The goal of this study was to construct a design methodology for a prosthesis which causes less stress shielding and meets fatigue requirements. Stress shielding is the reduction in bone stresses due to the introduction of an implant. Implants may become loose when stress shielding is present because bone resorption occurs as the bone adapts to the reduced bone stresses. Topology and lattice optimization were performed using OptiStruct to design a hip prosthesis where stress shielding and prosthesis fatigue were considered. The optimized design reduced stress shielding by 50+% when compared to a conventional generic implant, and the fatigue life met the ISO standards. Additionally, manufacturability was considered in the design process and a Ti-6Al-4V prototype was printed with an EOS selective laser melting machine.

BACKGROUND

In a total hip arthroplasty (THA), arthritic bone ends and damaged cartilage are removed and replaced with a hip implant. Over 800,000 total hip replacements are performed worldwide annually [1]. Total hip arthroplasty is one of the most clinically successful surgeries and improves quality of life for debilitating hip disease patients [2]. Nevertheless, 10-20% of the operations undergo a revision surgery [3], where risk is especially high for elderly patients. One of the common reasons of a revision surgery is loosening of the stem [2], which can be caused by bone resorption. Bone resorption also increases the bone fracture risk and makes revision surgery more complex.

Naturally, the femur carries load from the femoral head through the femoral neck to the cortical bone of the proximal femur. Most hip prostheses are made of solid metal and are stiffer than femur bone, so the implant takes a portion of load away from bone and reduces the stress in it. This is called stress shielding. Per Wolff's Law, bone remodels itself to adapt to external loading [3]. Bone resorption and degeneration can occur since the load through it is reduced.

Several studies have tried to solve the stress shielding issue. Ridzwan and Shuib proposed a topology optimized hip implant stem to reduce stress shielding [4]. They minimized compliance with different stem volume fraction constraints and chose the topologies that are feasible to interpret and manufacture. Comparing to a non-optimized implant, a 17% stress shielding reduction was achieved. However, their optimization setup produced the stiffest design within the specified amount of material, which was not ideal for reducing stiffness.

Recent advances in selective laser melting have made printing controlled lattice feasible. Khanoki and Pasini described a graded cellular hip implant by multiscale and multiobjective optimization [5]. They created macroscopic model with blocks and microscopic model with unit square cell. The design variable was cell porosity and the objectives were to minimize bone loss and minimize interface stress. Although this research considered material strength, it did not consider fatigue. The problem was reduced to a 2D design space with homogenous isotopic bone material model, which oversimplifies the 3D nature of the structure and loading.

This study proposes a methodology for designing solid-lattice hip implant to reduce stress shielding. A solid-lattice implant can be tailored with varying lattice beam diameters, which allows tuning stiffness and strength. The optimized implant will be compared with a generic conventional implant (generic implant). The geometry of this generic implant was based on the Smith & Nephew Synergy Titanium Ti-6Al-4V cementless size 14 standard offset porous-coated stem.

METHODS

A finite element method was applied to investigate stress shielding and to optimize an implant design (Fig. 1). Three models were constructed: intact femur model, femur with generic implant model, and femur with optimized implant model. Topology optimizations were performed using the generic implant as design space. The lattice and solid zones were determined by topology results, based on which a solid-lattice implant model was constructed. Diameter of each lattice beam/ligament was optimized by lattice optimization. Finally, stress shielding was evaluated and compared.

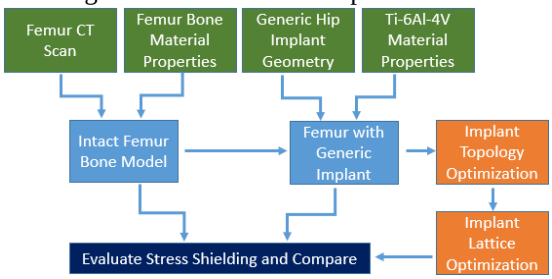

Figure 1: Hip implant design and optimization process

Models

Intact femur model: A femur bone's mechanical properties are neither homogeneous nor isotropic. It consists of a layer of cortical bone on the outer surface, and cancellous bone or spongy bone in the inner space. There is a cavity in the femur shaft filled with white marrow. A CT scan [6] and a 3D CAD of femur [7] were used to capture the geometry and to distinguish cortical bone and cancellous bone. The model was built and solved with Altair HyperWorks 14.0. Figure 2 shows the intact femur model and a cross-section view.

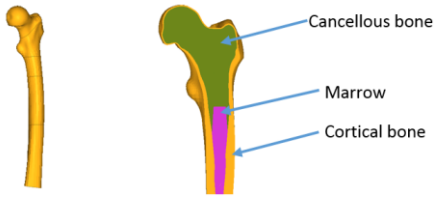

Figure 2: Femur bone model and cross-section view

Femur with generic implant model: The intact femur model was sectioned near the greater trochanter to mimic a standard femoral neck resection and the implant was positioned into it. This represents the structural configuration after a total hip arthroplasty, as shown in Fig. 3. Freeze contact, where the slave node is fixed relative to the master surface, was used to bond the implant head onto the implant stem. This has little effect on the bone stresses. The implant stem was fixed to the femur bone also by freeze contact. In reality, this is an interference fit and surgeons drive the stem into the tighter pre-trimmed cavity. However, Dammak and Shirazi-Adl studied the influence of interface simplifications, and showed that the stress distributions were similar between different friction coefficients and perfect bond case [8]. Thus, freeze contact was used to bond the implant stem and femur bone to simplify the problem and to reduce optimization time.

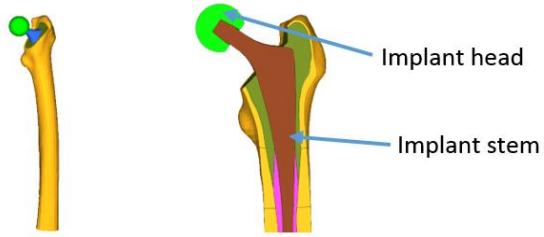

Figure 3: Femur with generic implant & cross-section view

Material Properties

All the materials in the finite element model were idealized as isotropic materials except for the cortical bone, which was modeled as an orthotropic material and is explained in Fig. 4. Table 1 shows the various sections of the finite element model and their material properties [9]. The stiffer direction (E1) of the orthotropic cortical bone aligned with the load path, as shown in the Fig. 5.

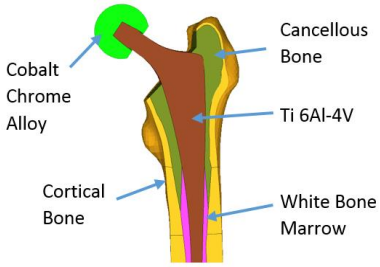

Figure 4: Material assignment in FE Model

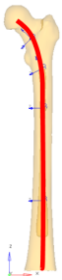

Figure 5: Red line shows cortical bone E1 direction

Table 1: Material Properties According to References [9][10]

Sections	Material	Modulus of Elasticity (GPa)	Poisson's Ratio (mm/mm)	Density (g/cm^3)
Implant Head	Cobalt Chrome Alloy	220	0.30	8.29
Implant Stem	Ti-6Al-4V	114	0.30	4.51
Spongy Bone	Cancellous (Spongy) Bone	1.00	0.30	0.45
Marrow	White Bone Marrow	0.30	0.45	1.00
Outer Femur Layer	Cortical Bone	E1=17.0 G12=3.30 E2=11.5 G23=3.60 E3=11.5 G31=3.30	μ_{12}=0.58 μ_{13}=0.31 μ_{23}=0.31	1.80

Loads and Boundary Conditions

Load cases from a study were used, which characterized femur loads for standing-up, standing, going up stairs, and jogging [11]. A combined load case was also considered [12]. Table 2 summarizes the load conditions. The lower truncated face of the femur was fixed for all load cases, as shown in Fig. 6. Lastly, two ISO Standard load cases (ISO7206-4 and ISO7206-6) were included to ensure the design has good fatigue strength. The implant was positioned and fixed per the ISO standards [11] (Fig. 7).

Table 2: Load case force summary table

Load Case (LC)	Location	Fx	Fy	Fz
Combined (LC1)	Head	262	-36	-681
	Abductor	-103	0	282
	Iliopsoas	-29	136	127
	Vastus Lateralis	0	0	-292
Standing Up (LC2)	Head	650	204	-1,428
Standing (LC3)	Head	576	121	-1,947
Stairs Up (LC4)	Head	712	657	-2,000
Jogging (LC5)	Head	774	771	-2,852
ISO (Stem)	Head	0	0	-2,300
ISO (Neck)	Head	0	0	-5,340

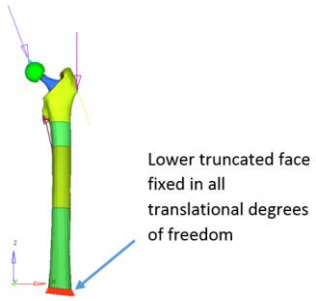

Figure 6: Combined Load Case

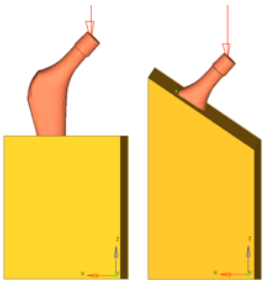

Figure 7: ISO Stem (left) and ISO Neck (right) Tests

Stress Shielding Measurement

To evaluate stress shielding, changes in strain energy or stress need to be measured. Weinans and Sumner defined the stress shielding as the change in strain energy (SE) after introducing the implant, as defined in Eq.1 [13]. Strain energy has equivalent meaning as "Compliance" in the solver and optimizer OptiStruct. Hence, compliance was used to measure stress shielding in this study. Fraldi and Esposito used Von Mises stresses to assess stress shielding because it is a non-negative value that indicates stress level [14]. They defined "Stress Shielding Increase" (SSI) by Eq. 2-4, where $\sigma^{\text{pre-THA}}$ and σ^{THA} are stresses before and after total hip arthroplasty for each element in the femur, and V^e is the volume of femur. Smaller SSI value means less stress shielding.

$$Stress\ shielding = \frac{SE\ (with\ implant) - SE\ (intact\ femur)}{SE\ (intact\ femur)} \quad \text{Eq.1}$$

$$SSI = \frac{<\sigma^{\text{pre-THA}}> - <\sigma^{\text{THA}}>}{<\sigma^{\text{pre-THA}}>} \quad \text{Eq.2}$$

$$<\sigma^{\text{pre-THA}}> = \frac{1}{\sum_e V^e}\sum_{V^e}\int_{V_e}(\sigma^{\text{pre-THA}})^e dV \quad \text{Eq.3}$$

$$<\sigma^{\text{THA}}> = \frac{1}{\sum_e V^e}\sum_{V^e}\int_{V_e}(\sigma^{\text{THA}})^e dV \quad \text{Eq.4}$$

Fatigue Strength

For ISO 7206-4 and ISO 7206-6 fatigue tests, the implant needs to survive 10^7 cycles. [11] Liu and Ouyang showed that the material of the implant, Ti-6Al-4V, can last 10^7 cycles with 680MPa stress [15]. This stress value was used as a design criterion for the optimization.

Topology Optimization

Design space: The generic implant stem, except for the neck region, was used as the design space. The interface between implant and environment was maintained, ensuring compatibility with current surgical tools.

Constraints: Research has shown that the cortical bone of the upper femur suffers the most severe stress shielding, and thus strain energy of that region was investigated [9]. To control the stress distribution better, regional compliance was used. The upper portion of femur cortical bone was divided into "Femur Head" and "Upper Shaft" sections (Fig. 8). OptiStruct restricted each section's regional compliance to be within 5% of that in the intact femur model. Volume fraction V_f less than or equal to 10%, 20%, and 30% were studied too.

Objective: Minimizing global compliance was used as the objective to obtain the most efficient structure.

Manufacturing constraints: Draw and extrusion constraints were applied to some of the studies to help understand and interpret the topology results.

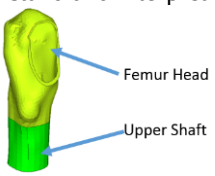

Figure 8: Femur Head and Upper Shaft

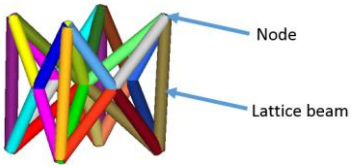

Figure 9: Face and Body Centered Cubic with Vertical Struts Unit Cell

Lattice Optimization

Solid-lattice model generation: Solid material zones were interpreted from the topology optimizations results, which are represented with shell and tetra elements. Semi-dense regions of the topology were filled with lattice by OptiStruct. Face and body-centered cubic with vertical struts (FBCCZ) unit cells (Fig. 9) were chosen because Leary and Mazur showed that it was one of the strongest printable cells [16]. The design will be printed in the vertical direction, so the beams' overhang angles are less than 45°, which ensures manufacturability. The unit cell size is 4-7mm, varying across the implant. The lattice was constructed with 1D beam elements since their diameters can be easily parameterized with OptiStruct.

Design variables: The design variables were the diameters of the lattice beams. The lattice beam could be tapered and have different diameters at the two ends. However, all beam ends need to have the same diameter at the joining node. Thus, the diameter at each joining node is an independent design variable. Based on the manufacturability and cell size, beam diameter can vary from 0.5mm to 2.0mm. Part of the skin shell thickness can vary between 0.5mm to 5.0mm.

Constraints: The fatigue strength requirement was found to be the most challenging criterion. Therefore, the standard ISO7206-4 load was used for lattice optimization, requiring that the von Mises stress of the implant should be no greater than 600MPa to have a safe margin.

Objective: Minimizing total volume was set as the optimization objective to save material and printing time.

RESULTS

Topology Optimization Results and Interpretation

Solid regions and lattice regions were determined by interpreting common feature of different optimization results. Figure 10 shows four topology results, which indicate the neck area of the stem is important, but the bottom half of the stem is undesired. Also, skin layer of solid material on the medial side and lateral side could be necessary. The difference in the optimization setup is summarized in Table 3.

Table 3: Optimization Parameters for Four Studies

	a	b	c	d
Volume fraction	<= 15%	<= 20%	<= 30%	<= 30%
Manufacturing Constraint	None	None	Split draw in lateral direction	Extrusion in lateral direction

A solid-lattice design of the implant stem was proposed in Fig. 11. The bottom tip was made solid with a smooth surface to aid in implant installation and to prevent bone ingrowth in that region, which may cause pain.

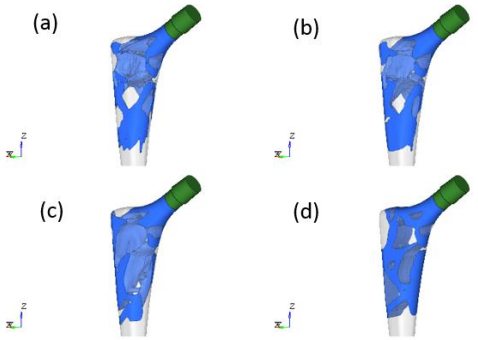

Figure 10: Topology Results Proposed Skin on Medial Side

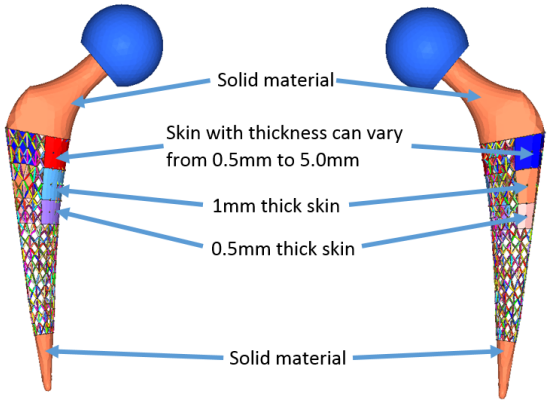

Figure 11: Solid Lattice Implant Design Space - Side Views

Lattice Optimization Results

The optimized solid-lattice implant (optimized implant) can reduce stress shielding effectively, and satisfy ISO fatigue requirements. Figure 12 compares upper cortical bone stresses between intact femur (left), femur with generic implant (middle), and femur with optimized implant (right) for LC4 as an example. With the optimized implant, the upper cortical bone stress distribution pattern was maintained and the bone stresses were closer to the intact femur stresses in magnitude, indicating that stress shielding is reduced.

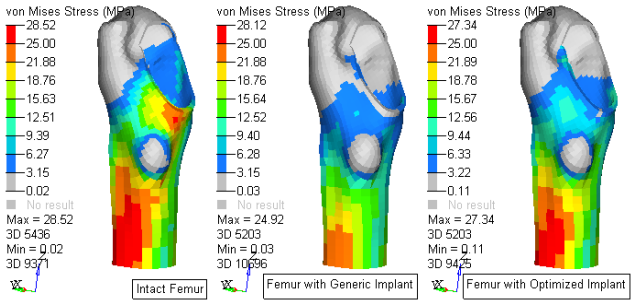

Figure 12: Stress Shielding is Reduced with Optimized Implant under Stairs Up Load (LC4)

To quantitatively evaluate stress shielding reduction, regional compliances and SSI were compared between generic implant and optimized implant. Figure 13 shows that the femur with the optimized implant has loadcase-average regional compliance that is 50.7% closer to that of the intact femur, when comparing to the generic implant. Figure 14 shows the optimized implant leads to an average of 57.3% lower SSI value over the five load cases than the generic implant, which agrees with the conclusion drawn using regional compliance measurements.

The optimized implant was validated against ISO7206-4 and ISO7206-6 load cases, where the maximum stress is 575MPa, which is lower than the endurance limit stress, indicating the optimized implant meets the fatigue standard.

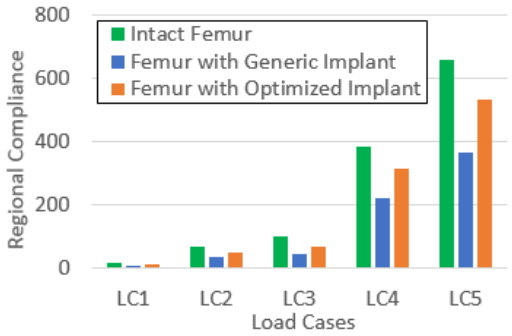

Figure 13: Regional Compliances of Intact Femur, Femur with Generic Implant, and Femur with Optimized Implant

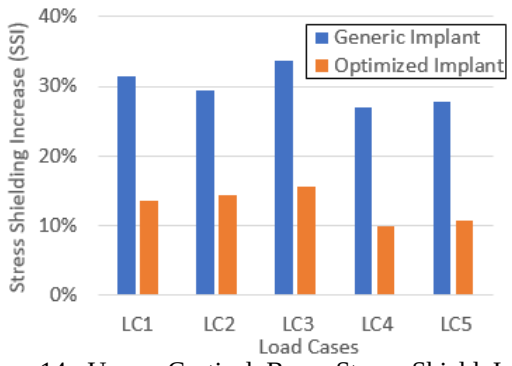

Figure 14: Upper Cortical Bone Stress Shield Increase with Generic Implant and Optimized Implant

INTERPRETATION

Through the optimization driven design process, the optimized implant reduced the stress shielding by more than 50% compared to the generic implant and can survive more than 10^7 life cycles. A Ti-6Al-4V prototype was printed with EOS M290 printer to prove the manufacturability, as shown in Fig. 15.

In the short term, this methodology can be applied to design standard prostheses. In the long term, customized prostheses can be designed and printed with each patient's femur geometry and bone material properties that are captured by Quantitative Computed Tomography, achieving the optimum treatment outcomes for each individual.

Micro-structure is controllable with 3D printing. Studies showed that porosity, pore size, and interconnectivity of the implant have influence on bone in-growth [17]. The micro-structure on the implant-bone interface can be designed and printed without an additional manufacturing process.

Nevertheless, there are some limitations for this study. Bone-implant interface is one of the main causes of aseptic loosening, and should be considered in future researches. Unit cell size and cell type were chosen based on experience, but those can be optimized as well. The final optimized implant is a conceptual design, and some detail design work is required before manufacturing.

Figure 15: EOS Printed Titanium Solid-Lattice Hip Implant

ACKNOWLEDGMENTS

The authors gratefully acknowledge the support and funding provided by Altair Engineering for the research and development of this paper. Additionally, we would like to thank EOS for printing our solid-lattice hip implant prototype so we could prove the manufacturability and better illustrate the results.

REFERENCES

[1] Li, C., Granger, C., Schutte, D., Biggers, S., Kennedy, J., & Latour, R. 2003, "Failure analysis of composite femoral components for hip arthroplasty," Journal of Rehabilitation Research and Development, 40(2), pp. 131-146.

[2] Bozic, K., Kurtz, S., Lau, E., Ong, K., Vail, T., & Berry, D. 2009, "The Epidemiology of Revision Total Hip Arthroplasty in the United States," The Journal of Bone and Joint Surgery(91), pp. 128-133.

[3] Ridzwan, M., Shuib, S., Hassan, A., Shokri, A., & Ibrahim, M. 2007, "Problem of Stress Shielding and Improvement to the Hip Implant Designs: A Review," Journal of Medical Sciences, 7(3), pp. 460-467.

[4] Ridzwan, M., Shuib, S., Hassan, A., Shokri, A., & Ibrahim, M. 2006, "Optimization in Implant Topology to Reduce Stress Shielding Problem," Journal of Applied Sciences, 6(13), pp. 2768-2773.

[5] Khanoki, S., & Pasini, D. 2012, "Multiscale Design and Multiobjective Optimization of Orthopaedic Hip Implants with Funcionally Graded Cellular Material," Journal of Biomechanical Engineering, 5, pp. 935-944.

[6] Gaillard, F, "Multiple Myeloma – Femur," Last modified January 20, 2012, accessed September 28, 2016, https://radiopaedia.org/cases/multiple-myeloma-femur

[7] IA, "Femur," last modified May 8, 2012, accessed September 22, 2016, https://grabcad.com/library/femur

[8] Dammak, M., Shirazi-Adl, A., & Zukor, D. J. 1997, "Analysis of cementless implants using interface nonlinear friction-Experimental and finite element studies," Journal of Biomechanics, 30(2), pp. 121-129.

[9] Noyama, Y., Miura, T., Ishimoto, T., Itaya, T., Niinomi, M., & Nakano, T. 2012, "Bone Loss and Reduced Bone Quality of the Human Femur after Total Hip Arthroplasty under Stress-Shielding Effects by Titanium-Based Implant," Materials Transactions, 53(3), pp. 565-570.

[10] Reilly, D. T., & Burstein, A. H. 1975, "The elastic and ultimate propreties of compact bone tissue," J. Biomechanics, (8), pp. 393-405.

[11] Bergmann, G., Bender, A., Dymke, J., Duda, G., & Damm, P. 2016, "Standardized Loads Acting in Hip Implants," PLoS One https://doi.org/10.1371/journal.pone.0155612.

[12] Simones, J., Vaz, M., Blatcher, S., & Taylor, M. 2000, "Influence of head constraint and muscle forces on the strain distribution within the intact femur," Med Eng Phys(22), pp. 453-459.

[13] Weinans, H., Sumner, D., Igloria, R., & Natarajan, R. 2000, "Sensitivity of periprosthetic stress-shielding to load and the bone density-modulus relationship in subject-specific finite element models," Journal of Biomechanics, 33(7), pp. 809-817.

[14] Fraldi, M., Esposito, L., Perrella, G., Cutolo, A., & Cowin, S. 2010, "Topological optimization in hip prosthesis design. Biomechanics and Modeling in Mechanobiology," 9(4), pp. 389-402.

[15] Liu, Y., Ouyang, Q., Tian, R., & Wang, Q. 2009, "Fatigue Properties of Ti-6Al-4V Subjected to Simulated Body Fluid," Tech Science Press, 2(3), pp. 169-175.

[16] Leary, M., Mazur, M., Elambasseril, J., McMillan, M., Chirent, T., Sun, Y., Qian, M., Easton, M., Brandt, M. 2016, "Selective laser melting (SLM) of AlSi12Mg lattice structures," Materials and Design, 98, pp. 344-357.

[17] Wang, X., Xu, S., Zhou, S., Xu, W., Leary, M., Choong, P., Qian, M., Brandt, M., Xie, Y. 2016, "Topological design and additive manufacturing of porous metals for bone scaffolds and orthopedic implants: A review," Biomaterials, 83, pp. 127-141.